AIAA JOURNAL
Vol. 48, No. 10, October 2010

Applications of Actuator Disk Theory to Membrane Flapping Wings

Sergey Shkarayev* and Dmytro Silin†
University of Arizona, Tucson, Arizona 85721

DOI: 10.2514/1.J050139

This study addresses the aerodynamics of elastic membrane flapping wings. Several applications of the actuator disk theory to the flapping wings of insects and birds are reviewed. In previous studies, to account for spatial and temporal variance in the wake behind the flapping wings, empirical corrections were proposed for the induced velocity and power. In the present paper, a new procedure for determination of the correction factor is proposed, using membrane-type flapping-wing devices. Wind-tunnel experiments were conducted and the stroke-averaged propulsive thrust was measured on 25-cm-wingspan (flat and 9% camber) and 74-cm-wingspan flapping-wing models. Either flapping frequency or input power was held constant during the tests. Obtained thrust forces were compared to theoretical values predicted by the actuator disk theory. Empirical correction factors to the actuator disk theory were determined, providing a best fit to the experimental data when the flapping axis aligned with freestream velocity. It is noteworthy that the numerical value for the correction factor for the 25 cm cambered wing agrees with the results obtained on large insects. The theoretical corrections for angle of attack of the flapping wing give satisfactory agreements with the experimental data only for relatively low forward speeds.

Nomenclature

A	=	area of actuator disk, $\Phi b^2/4$
b	=	tip-to-tip wingspan of flapping wing, $2R$
C_{T0}	=	thrust coefficient without freestream
c	=	chord length
d	=	propeller diameter
f	=	flapping frequency
h	=	maximum height of the airfoil
k	=	correction factor
$\mathbf{n}$	=	flapping axis
q	=	dynamic pressure
P	=	induced power
P_e	=	input electric power
R	=	length of wing
S	=	wing (blade) surface area
T	=	thrust force
V	=	freestream velocity
w	=	induced velocity
w_e	=	experimental value of induced velocity
z	=	distance from propeller disk
α	=	angle of attack of flapping wing
β	=	angle of actuator disk
Φ	=	flapping amplitude
ρ	=	air density
0	=	subscript referring to test conditions without freestream

I. Introduction

THE motion of a membrane flapping wing includes articulated rotations of its base as a rigid body and elastic bending and twisting deformations. The aerodynamics of flapping wings is a combination of several complex phenomena, including Wagner effects, wake capture, leading edge vortex, near fling, and added mass. Results of recent experimental and theoretical investigations of flapping flight have been covered in reviews underlying fluid mechanics and aerodynamics [1–3], flapping flight controls [4], and theoretical and numerical modeling of unsteady flowfields in the near and far wakes of oscillating wings [5,6].

The aerodynamic theory of rotors, propellers, and ducted fans [7,8] is based on the blade element theory and the actuator disk theory. The classical actuator disk theory provides an understanding of the performance of rotors, propellers, and ducted fans and relates their performance to simple design parameters. In the actuator disk theory, originally developed by Rankine [9] and Froude [10], the disk axis of rotation is placed at a zero angle of attack with respect to the freestream. Applying the momentum theorem to a control volume surrounding the disk, the analytical relation was established between the wake velocity and thrust force generated by a given induced power to the actuator. The zero-angle-of-attack constraint may be applicable to vertical flights or hovering for rotorcraft. Glauert [11] extended the actuator disk theory for a general flight case of the arbitrary angle of attack. This theory was found to be well suited for analysis and design of airplane propellers and rotors under conditions of axial symmetry in the air flow.

In early investigations, the similarities of flapping wings and propellers were noted, giving argument for an application of the steady aerodynamic theory to flapping-wing animals. Osborne [12] hypothesized that a flapping wing, at a given time instant, moving with some instantaneous velocity and angle of attack generates the same amount of instantaneous thrust and lift as a rigid blade element moving at the same constant velocity and angle of attack. Combining the blade element analysis with the axial momentum theory, stroke-averaged forces were determined over a wing stroke [12]. The values of the vertical and horizontal components of the total force were compared to the weight of flying animals and generated thrust, respectively. Average lift and drag coefficients were computed and the applicability of this quasi-steady aerodynamic model to fast horizontal flight was reasonably well proven. However, this method did not provide reliable estimates for aerodynamic forces in a slow flight or in a hover.

Pennycuick [13] synthesized a theoretical model of the power required for birds in horizontal flight. In this treatment, the induced power and lift required to support the weight in a horizontal flight were determined using a momentum equation. This equation can be derived as an approximation of the actuator disk theory [11] for

Presented as Paper 2009-0878 at the 47th AIAA Aerospace Sciences Meeting, Orlando, FL, 5–8 January 2009; received 17 August 2009; revision received 30 June 2010; accepted for publication 15 July 2010.

*Associate Professor, Department of Aerospace and Mechanical Engineering, 1130 North Mountain Avenue. Senior Member AIAA.

†Graduate Research Assistant, Department of Aerospace and Mechanical Engineering, 1130 North Mountain Avenue.

high-speed horizontal flight. To account for deviations of the ideal from the real unsteady flowfield, the ideal induced power was multiplied by an empirical factor of 1.2.

Ellington [14] modified the actuator disk theory by introducing a model of the partial actuator disk, which is obviously a better model for flapping wings having a flapping amplitude less than 180 deg. In this model, the disk area is defined as a projection of the area swept by flapping wings on the horizontal plane. Since the Rankine–Froude theory assumes a uniform and continuous velocity distribution at any cross section of the control volume, Ellington [14] further modified the theory by including nonuniform pressure distributions. Such modification was applied to a hovering flight, providing a spatial correction to the theory. A temporal correction to the actuator disk theory was developed by introducing pressure pulsations of frequency equal to the frequency of flapping. These two modifications were combined in one correction factor, which was eventually applied to the induced velocity and power in thrusting flapping wings in hover conditions. It was shown that this correction factor must be greater than unity. Willmot and Ellington [15] used this correction to the wake velocity in a model for the mean lift coefficient and associated power components in insects in horizontal flight.

Sunada and Ellington [16] proposed a method for estimating and explaining aerodynamic forces in flapping wings based on added masses in vortex sheets. Comparisons of numerical results obtained by this method and by the modified actuator disk theory were conducted for several insects and birds. They showed that the correction factor actually can be in the wider range of 1.2–2.2.

For the majority of flight regimes, aircraft performance can be accurately described by averaged quantities, such as velocities, angle of attack, aerodynamic forces, and powers. This argument was used for the applications of momentum equations to study the performance of flapping wings [17].

In previous studies [12–17], corrections to the actuator disk model were applied extensively to compensate for deviations of evenly distributed velocity in the downwash for the model and a real, unsteady flowfield behind the flapping wings. However, the values of this factor were estimated from measurements on flying species. A digital image correlation technique was employed in [18] to measure downwash velocity distribution at the midstroke of a tethered desert locust. Using these data, the value of the correction factor was found to be 1.12, suggesting only a 12% loss of induced power by the locust wings in comparison to the ideal actuator disk.

Actuator disk theory is a relatively simple analytical treatment of the propulsive thrust and power. So far, substantial quantitative data have been obtained by applications of the theory to flying insects and birds. However, these data suffer uncertainties inherent to experiments on flying species. Unlike a biological system, flapping-wing aerodynamics can be studied explicitly on man-made flapping wings, since the input parameters specifying their kinematics and structures can be placed under full experimenter control.

The objectives of the present study are to investigate propulsive thrust generation by flapping wings featuring an elastic membrane attached to the spar and stiffened by battens. In this paper, the thrust forces are measured in a wind tunnel under conditions of constant input power or constant flapping frequency. Comparisons are drawn between obtained data and the actuator disk theory, and results are used in the estimates of a correction factor to the actuator disk theory.

II. Application of Actuator Disk Theory to Flapping Wings

The kinematics of flapping wings is a complex phenomenon that is mainly responsible for their exceptional flight performance characteristics. The membrane wing structure is flexible and characterized by flexural and torsional stiffness. The main kinematic parameters of the wing motion are positional angle, rotational angle about its longitudinal axis, and a phase angle shift between flapping and rotational oscillations of the wing.

The motion of the flapping wing is described with respect to the flapping plane, also called a stroke plane in Fig. 1. This plane is formed by the utmost upstroke wingtip position (point U), downstroke wingtip position (point D), and the wing base (point O). Aerodynamic forces developed by flapping wings depend mainly on the angle of attack α, flight velocity V, flapping frequency f, wing angular velocity, and flexural and torsional stiffness. The angle of attack of the flapping wings is defined as the angle between the freestream velocity and the flapping axis, **n**, as can be seen in Fig. 1.

The real flow around and in the wake of the flapping wings is unsteady. To apply actuator disk theory to flapping wings, the wings are replaced with an infinitely thin disk. The assumptions are made that the fluid is ideal and the flowfield parameters are averaged over the time of one flapping stroke. Then a one-dimensional axial momentum balance can be applied to the actuator disk.

The actuator disk can be placed at some angle β with respect to the freestream, which may or may not be equal to α. The direction of the thrust force T is normal to the actuator disk (Fig. 1). For an arbitrary β, the relation between the thrust force and the velocity w, induced in the flow passing the disk, is given by [11]

$$T = 2\rho A w V' \tag{1}$$

where V' is a resultant velocity, which is a geometric sum of forward and induced velocities:

$$V' = \sqrt{(V\cos\beta + w)^2 + (V\sin\beta)^2} \tag{2}$$

For the flapping wings, the partial disk area should be used as a projection of the area swept by flapping wings on the stroke plane (Fig. 1) [14]:

$$A = \Phi b^2/4 \tag{3}$$

In Pennycuick's [13] theoretical model of the power required for horizontal flight of birds, the induced velocity was determined directly from Eq. (1) assuming $V' = V$, so that $w = T/(2\rho AV)$. This formula implies that $\beta = 90^\circ$ and $V \gg w$ in Eq. (2). To account for any deviations from the ideal flowfield, the ideal induced power in that study was multiplied by an empirical correction factor.

Substituting Eq. (2) into Eq. (1), the induced velocity at the actuator disk can be found from the quartic equation:

$$w^4 + 2w^3 V\cos\beta + w^2V^2 = \left(\frac{T}{2\rho A}\right)^2 \tag{4}$$

The ideal power required by flapping wings is a product of the thrust and the projection of the velocity on the normal to the actuator disk:

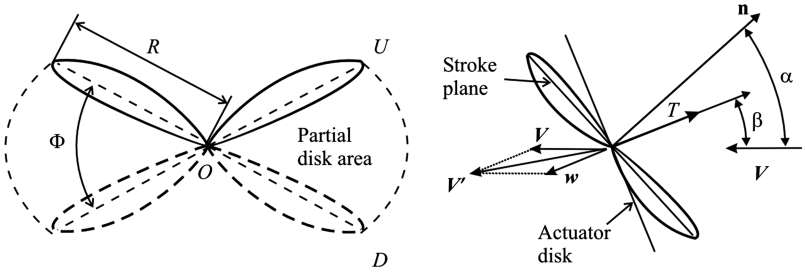

Fig. 1 Schematics of flapping wings (left) and actuator disk model (right).

$$P = T(V\cos\beta + w) \tag{5}$$

The hovering flight corresponds to the condition of $V = 0$. Then Eqs. (4) and (5) reduce to the results of Rankine–Froude theory:

$$w_0 = \sqrt{\frac{T_0}{2\rho A}} \tag{6}$$

$$P_0 = T_0 w_0 \tag{7}$$

Using w_0 as the reference velocity, Eq. (4) is nondimensionalized and written in the form [7]

$$\left(\frac{w}{w_0}\right)^4 + 2\left(\frac{w}{w_0}\right)^3\left(\frac{V}{w_0}\right)\cos\beta + \left(\frac{w}{w_0}\right)^2\left(\frac{V}{w_0}\right)^2 = \left(\frac{T}{T_0}\right)^2 \tag{8}$$

To account for the nonuniformity and time variance of the wake that eventually reduces the efficiency of the actuator disk, Ellington [14] proposed a correction to the hovering induced velocity of

$$w_{0C} = k w_0 \tag{9}$$

where k is the empirical correction factor. Substituting w_{0C} for w_0 in Eq. (8) we have

$$\left(\frac{w_C}{w_{0C}}\right)^4 + 2\left(\frac{w_C}{w_{0C}}\right)^3\left(\frac{V}{w_{0C}}\right)\cos\beta + \left(\frac{w_C}{w_{0C}}\right)^2\left(\frac{V}{w_{0C}}\right)^2 = \left(\frac{T}{T_0}\right)^2 \tag{10}$$

The solution of this equation gives a corrected induced velocity, w_C, in the case of nonzero freestream velocity. Thus, for the case of $\beta = 0°$, the induced velocity is found:

$$w_C = -0.5V + \sqrt{0.25V^2 + w_{0C}^2\frac{T}{T_0}} \tag{11}$$

According to the momentum theory, the ultimate change of the velocity in the far wake is $2w_C$ and corresponding dynamic pressure in the far wake is derived with the help of Eqs. (6) and (11) as a sum of the freestream dynamic pressure and the corrected disk loading:

$$q = 0.5\rho V^2 + k^2\frac{T}{A} \tag{12}$$

For horizontal flight with a near horizontal stroke plane, the actuator disk also can be placed horizontally ($\beta = 90°$). Then the thrust plays the role of the lift. For $\beta = 90°$, assuming constant thrust, Eq. (10) reduces to

$$w_C = \sqrt{-0.5V^2 + \sqrt{0.25V^4 + w_{0C}^4}} \tag{13}$$

This simple formula was used by Wilmot and Ellington [15] in studies of insect aerodynamics.

The corrected induced power is given by

$$P_C = T(V\cos\beta + w_C) \tag{14}$$

which is simplified for hovering (zero freestream velocity) as

$$P_{0C} = T_0 w_{0C} = k T_0^{3/2}/\sqrt{2\rho A} \tag{15}$$

From which it follows

$$k = w_{0C}/w_0 = P_{0C}/P_0 \tag{16}$$

Thus, for hovering, the correction factor k turns out to be the induced power efficiency of the flapping wings in hover.

For the case of constant induced power, by equating Eqs. (14) and (15), the following relation holds:

$$T(V\cos\beta + w_C) = T_0 w_{0C} \tag{17}$$

Solving Eqs. (10) and (17) simultaneously, the variation of thrust with forward speed for an arbitrary actuator disk angle can be found. In the particular case of $\beta = 0°$, from Eqs. (11) and (17), the following equation for T/T_0 in terms of V/w_{0C} is derived:

$$\frac{T}{T_0}\left(\frac{V}{2w_{0C}} + \sqrt{\frac{V^2}{4w_{0C}^2} + \frac{T}{T_0}}\right) = 1 \tag{18}$$

This equation will be used in the present study for the determination of the correction factor k based on the best fit of the theory to experimental data.

III. Experimental Setup

A. Wind-Tunnel Facility

Experimental studies were conducted on 25 cm (flat and 9% camber) and 74-cm-wingspan flapping-wing models. Flat wings were tested in the University of Arizona Wind Tunnel (Fig. 2). This wind tunnel has a 3×4 ft test section and a velocity range from 2 to 30 m/s. The flow is laminarized in a settling chamber to a turbulence level of less than 0.3% in the axial direction. A flapping-wing model installed in the tunnel is shown in Fig. 2.

The force balance used in this study contains six precision flexures with strain gauges for measuring lift, drag, side force, pitching, rolling, and yawing moments. For this sequence of tests, side force, rolling, and yawing moments were not sought. This is an external force balance located under the test section of the wind tunnel, as shown in Fig. 3.

Data from strain gauges were logged using two National Instruments SCXI-1321 terminal blocks in a low-noise SCXI-1000 chassis capable of sampling at 330,000 Hz. The nominal resolution of each flexure was about 0.004 N. The zero drift for flexures did not exceed 1.5% over 15 min of testing time with no load applied. When an oscillatory load was applied through the 25 cm flapping wings operating at 20 Hz, the zero drift for the same flexures did not exceed 2% per 15 min of testing.

To determine the error in the measured aerodynamic forces, calibration of the wind tunnel and the balance was performed before each test series. Using calibration measurements and the small-sample method [19], uncertainty intervals in aerodynamic forces corresponding to a confidence level of 90% were determined. For the range of measured forces 0–5 N, the uncertainty intervals were 0.015 N for vertical and 0.007 N for horizontal forces. The value of the lift channel uncertainty was higher because the lift was measured by two flexures; thus, two sources of measurement errors contributed to the total uncertainty. For the pitching moment of order 0–0.15 Nm, the uncertainty interval was of 0.0005 Nm. The standard deviation of

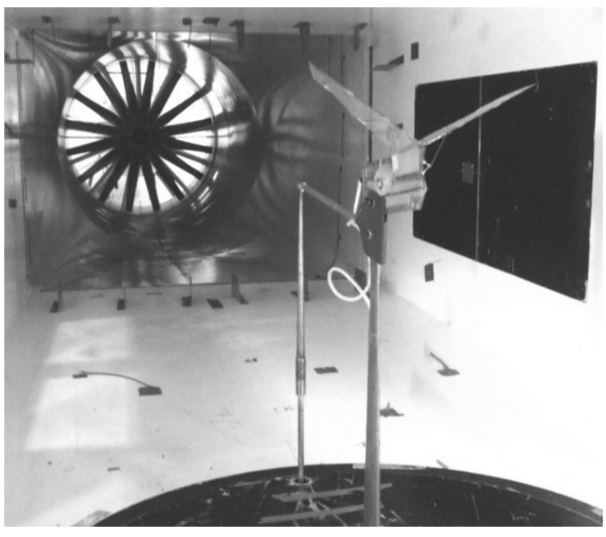

Fig. 2 Flapping-wing model in the wind tunnel.

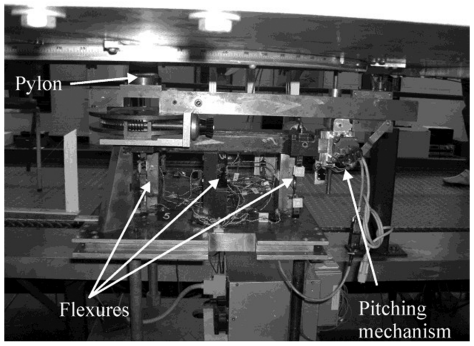

Fig. 3 Force balance.

measured dynamic pressure was 0.4 N/m^2 for the range of velocities studied in the present work.

Measurements on the cambered flapping wing were conducted in a low-speed wind tunnel located at the University of Florida's Research and Engineering Education Facility [20].

B. Flapping-Wing Models

Force measurements were conducted for two flapping-wing models of the 25 and 74 cm wingspans (Fig. 4). Each test model consists of a mounting rib, flapping wings, dc electric motor, and flapping transmission. Generic drawings of the wings are shown in Fig. 5. Geometrical and mass data for the flapping wings and transmission are presented in Table 1.

a) 25-cm flapping-wing model

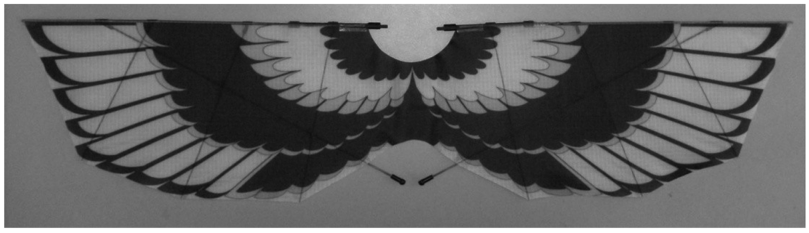

b) 74-cm flapping-wing model

Fig. 4 Flapping-wing models studied.

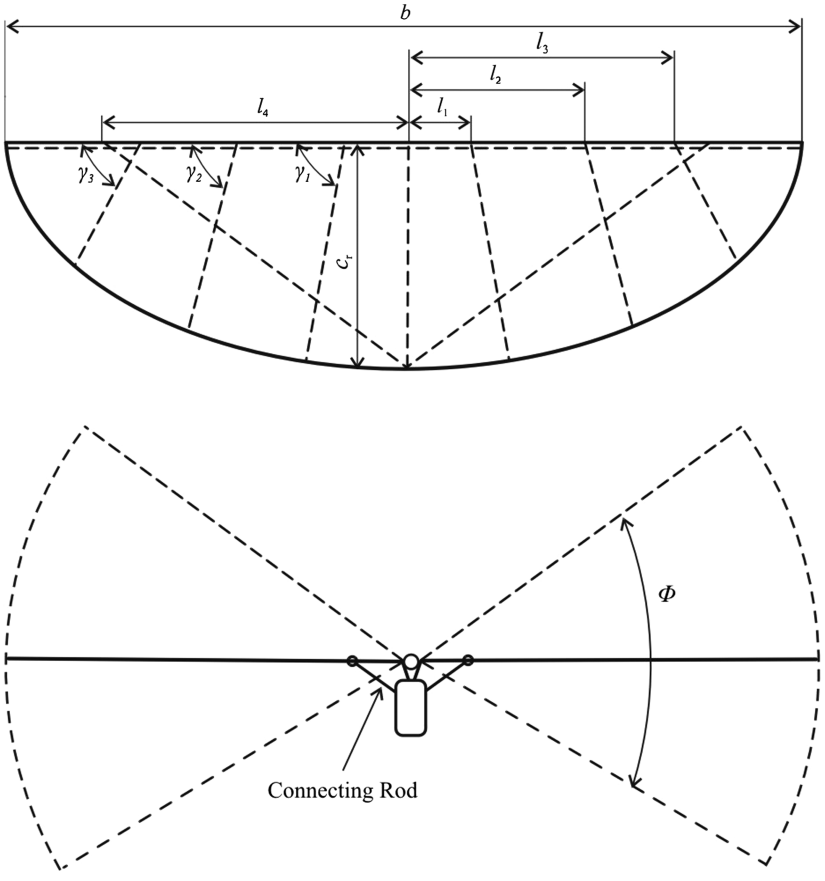

Fig. 5 Geometry of flapping-wing model.

Table 1 Specifications of flapping-wing models

Wing model	25 cm	74 cm
Wingspan b, cm	25	74
Flapping amplitude Φ, deg	72	55
Wing area S, cm^2	137	991
Batten 1, $l_1 \times \gamma_1$, cm × deg	3.8 × 75	7.5 × 80
Batten 2, $l_2 \times \gamma_2$, cm × deg	8 × 60	16.5 × 75
Batten 3, $l_3 \times \gamma_3$, cm × deg	——	25.5 × 65
Intersection point l_4, cm	——	27
Root chord c_r, cm	7	16.8
Wingtip deflection, cm/g	0.18	0.95
Mass, g	1.15	15.8
Motor type	Maxon Re-13	Speed-370
Gear ratio	8:1	64:1

The 25 cm wings were made in two variants: flat and cambered. The 9% camber airfoil was formed by connecting a segment of a parabola to a straight line. These lines are tangent at the connecting point (Fig. 6). The maximum height of the airfoil, h, is located at the quarter-chord point from the leading edge. The camber is expressed as a percentage of the ratio h/c, where c is the chord length. A camber in the flapping-wing model was introduced into the wing structure through the shaping of metal ribs.

The 25 cm wing structure consisted of wing arms, a front spar, four battens, and a membrane. Wing arms were made of 0.8 mm music wire. The membrane was 0.015 mm Mylar bonded to the front spar and battens with rubber cement. Pultruded carbon rods were used: T315-4 of 0.8 mm diameter for the front spar and T305-4 of 0.5 mm diameter for battens. Battens were not rigidly fixed to the front spar, allowing pitching deformations of the membrane caused by inertia and aerodynamic forces.

A wing from a commercial ornithopter, Cybird P2, was used as the 74 cm flapping-wing model. Its structure included front and rear spars, six battens, and a membrane made of nylon cloth. Battens were rigidly fixed to both front and rear spars.

IV. Experimental Results

A. Constant-Frequency Tests

Measurements on the 25 and 74 cm flapping-wing models were conducted in conditions with no freestream: i.e., $V = 0$. The models were mounted on the top of the pylon fixture of the aerodynamic balance and tested at varying flapping frequencies.

The conventional design and analysis of rotating wings is based on nondimensional coefficients. Similarly, the thrust coefficient for flapping wings can be defined in terms of average wingtip speed $V_T = f\Phi b$ and reference area S as

$$C_{T0} = \frac{T_0}{0.5\rho V_T^2 S} \tag{19}$$

Figure 7 shows the plots of thrust coefficients versus flapping frequency. The 90% confidence intervals shown in Fig. 7 were calculated from uncertainties presented in Sec. III.A and in [20].

Using data obtained by Singh and Chopra [21] for articulated wings (soft spring in Fig. 21a in [21]), thrust coefficients are calculated using formula (19). The wing has an area of 0.012 cm^2 and a pitch angle of $\pm 30°$. Thrust coefficients for this wing are also presented in Fig. 7. They are generally two–three times smaller than for the membrane wings in the present study.

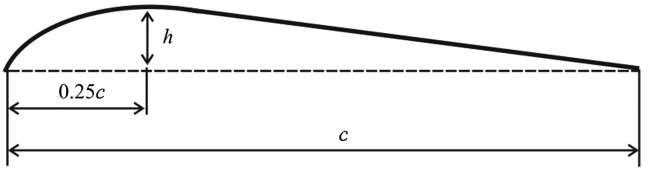

Fig. 6 Cambered airfoil.

The 25 cm flat and 74 cm wing plots exhibit a similar parabolic shape. The 25 cm cambered wing shows higher values of the thrust coefficient, especially at higher flapping frequencies (maximum of 0.84). Note that the thrust coefficient data for the cambered wing are fairly close to constant. The importance of camber in flapping wings was shown in recent experimental [20] and theoretical [22] studies. They reported higher lift and thrust for cambered wings in comparison with flat wings.

In early studies, some similarities in function and geometry were noticed in flapping wings and propellers. In the present study, both propellers and flapping wings are analyzed using the actuator disk model; therefore, thrust coefficients available for small propellers are also presented.

In a previous study [23], a propulsion system consisting of two coaxial contrarotating propellers of a diameter $d = 14$ cm (the area of four blades, $S = 0.003$ cm^2) and of a pitch 11.4 cm was investigated. The thrust force reaches the maximum of 3.42 N at 200 Hz. Corresponding thrust coefficient is 0.30 and has a very little (less than 5%) variation with frequency in the range of 60–200 Hz. (Remember that an average thrust coefficient of 0.34 was achieved for the articulated flapping wings [21].)

B. Constant-Power Tests and Comparisons with Actuator Disk Theory

A thrust force was measured in the wind tunnel with the input power to the electric motor, P_e, held constant. Numerical values of the inputted electric power, measured with no freestream, i.e., $V = 0$, thrust data, and corresponding flapping frequencies are presented in Table 2. The electric power was much higher for the cambered wings, which could be due to higher induced and profile drags on the cambered wings, and to higher electrical power losses in the motor.

In the first series of wind-tunnel experiments, the flapping axis was aligned with a freestream. It corresponds to the case of a zero angle of attack, $\alpha = 0°$. At a given input power, the freestream speed was varied at $V = 0$–6 m/s, with an increment of 1 m/s. Thrust values were obtained for three wing models and for all speeds. The induced velocity w_0 was found from Eq. (6) and ratios V/w_0 were calculated.

For the case of constant power, Eq. (18) can be used for determining the ratio of T/T_0 generated by the actuator disk at a given relative velocity V/w_{0C} if the correction factor k is known. In the present study, the method for the determination of k is proposed based on the best fit of experimental data to theory [Eq. (18)] in the least-squares sense.

A nonlinear least-squares problem was solved numerically for the parameter k varying from 1 to 3 in increments of 0.01. The best-fit value of the parameter k corresponds to the minimum of the sum of squared deviations of experimental values of T/T_0 from the theoretical values calculated from Eq. (18).

The values of the best-fit correction factor k were found to be 1.18, 1.81, and 2.68 for the 25 cm cambered, 25 cm flat, and 74 cm wings, respectively. When treating the parameter k according to Eq. (16) as

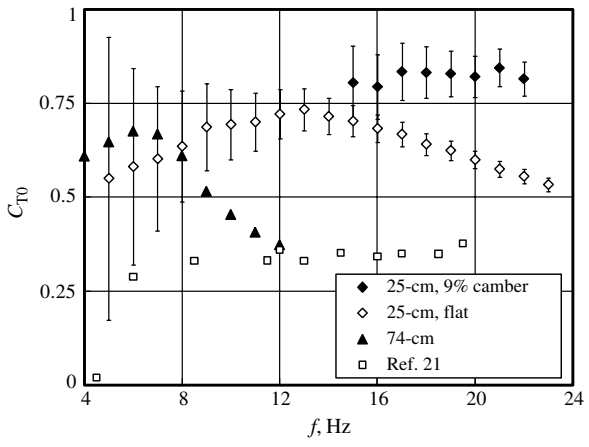

Fig. 7 Variation of thrust coefficient with flapping frequency.

Table 2 Input power, thrust, and flapping frequency

Wing model	74 cm			25 cm flat			25 cm cambered		
P_e, W	25	32.5	40	1	2	3	1.2	3.6	4.4
T_0, N	0.814	1.031	1.230	0.086	0.153	0.211	0.102	0.141	0.148
f, Hz	6.6	8.1	9.7	13	18	21	13	16	17

an induced power efficiency of the flapping wings in hover, the 25 cm cambered wing has the lowest induced power losses of 18% and highest thrust coefficient (Fig. 7). Thus, the 25 cm cambered wing shows much better induced power efficiency in comparison to the 74 and 25 cm flat wings. The implication of this result is that the initial geometry of a membrane wing plays an important role in its aerodynamic performance.

Using obtained values of the best-fit correction factor k, experimental data points of T/T_0 are plotted as functions of V/w_{0C} in Figs. 8–10; the theoretical curve of Eq. (18) is presented as well. Equation (18) implies that for the case of constant induced power, the thrust ratios are independent of the value of power. Despite some scatter, obtained experimental data show consistency with this theoretical result. As can be seen from these figures, the experimental data agree with the theory within a margin of error of $\pm 15\%$. It is worth noting that the data for the larger 74 cm wing are less scattered, which may be due to the higher measured values of thrust force for this wing.

In a previous study [23], a hot-wire system was used for measuring velocity profiles in the slipstream behind contrarotating propellers. Experimental data for velocity distributions w_{ei} are presented in Fig. 10 of [23] at the distance $z = 7$ cm from the propeller disk for two values of thrust: $T = 1.47$ and 2.45 N. In the present study, using these data, the average induced velocity at the distance z was calculated as

$$w(z) = (1/n)\sum_{i=1}^{n} w_{ei} \tag{20}$$

Then the experimental value of the induced velocity w_{0C} passing the disk was determined using formula (4-56) from [7] as

$$w_{0C} = w(z) \Big/ \left[1 + \frac{2z/d}{\sqrt{1 + (2z/d)^2}}\right] \tag{21}$$

Using this result, the value of the correction factor k was found from Eqs. (6) and (16): 1.07 and 1.03 for thrusts of 1.47 and 2.45 N, respectively.

Since the actuator disk theory does not take into account power losses associated with the parasite and profile drag components, the analysis of the obtained data is relevant only to the power induced by the actuator disk into the axial flow. It is noteworthy though that the numerical value for the correction factor for a 25 cm cambered wing (1.18) is close to the results obtained for the large insect (1.12[18]) and contrarotating propeller (1.03, 1.07).

Application of the momentum theory to the case of a nonzero angle of attack was investigated in the present study for the 25 cm flat wing. In the wind-tunnel experiments, the angle of attack was varied as $\alpha = 28$, 56, and 85°. Using results of measurements and the previously obtained value for the correction factor, plots of T/T_0 versus V/w_{0C} were generated and are presented in Figs. 11–13,

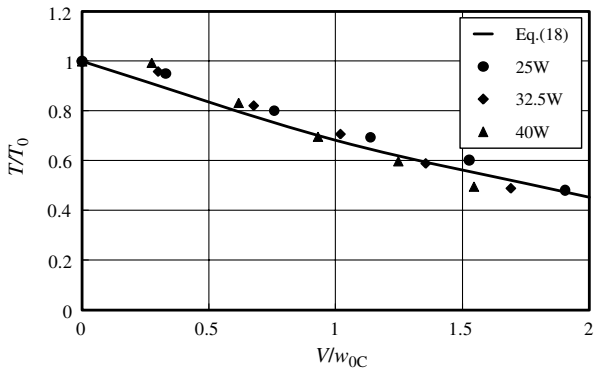

Fig. 8 Variation of thrust with speed for constant power: $b = 74$ cm, $k = 2.68$, and $\alpha = \beta = 0$ deg.

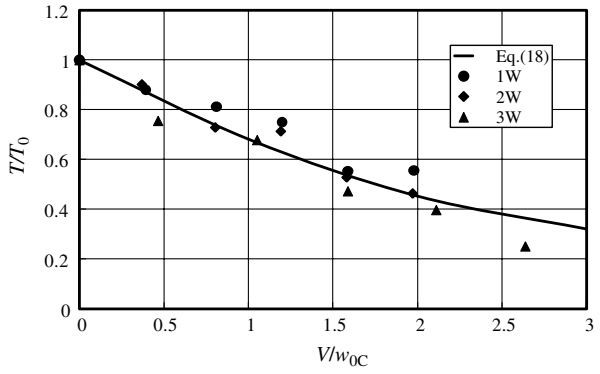

Fig. 9 Variation of thrust with speed for constant power: $b = 25$ cm, flat, $k = 1.81$, and $\alpha = \beta = 0$ deg.

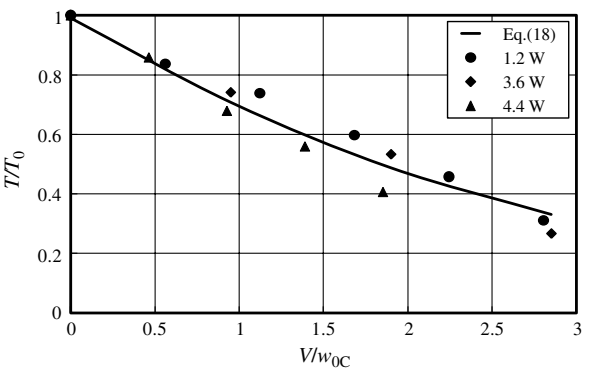

Fig. 10 Variation of thrust with speed for constant power: $b = 25$ cm, 9% camber, $k = 1.18$, and $\alpha = \beta = 0$ deg.

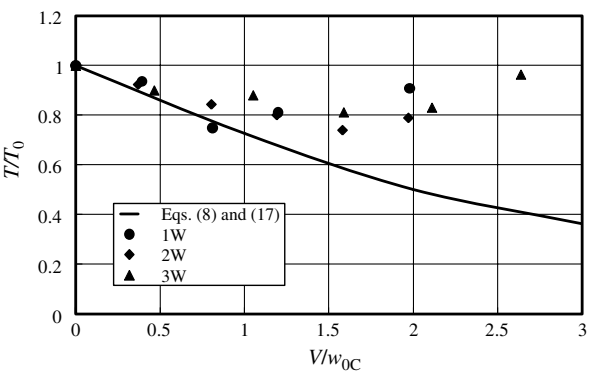

Fig. 11 Variation of thrust with speed for constant power: $b = 25$ cm, flat, $k = 1.81$, $\alpha = \beta = 28$ deg.

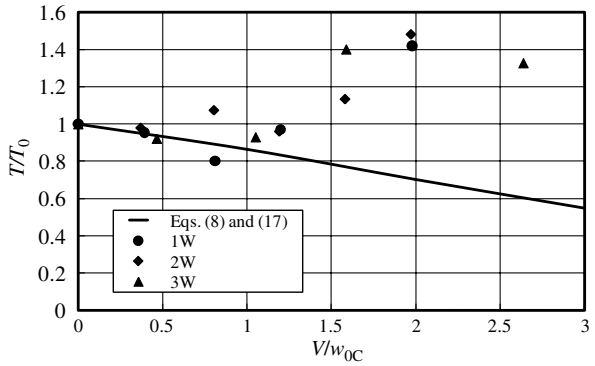

Fig. 12 Variation of thrust with speed for constant power: $b = 25$ cm, flat, $k = 1.81$, and $\alpha = \beta = 56$ deg.

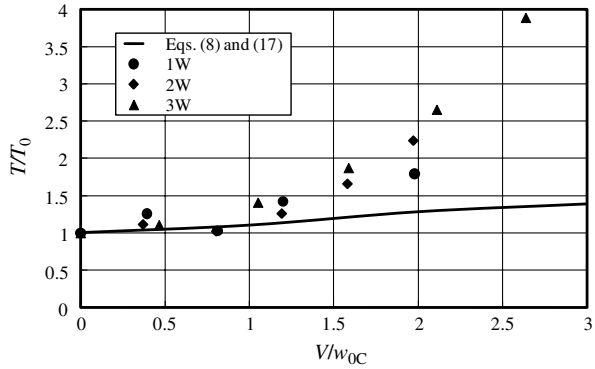

Fig. 13 Variation of thrust with speed for constant power: $b = 25$ cm, flat, $k = 1.81$, and $\alpha = \beta = 85$ deg.

together with the theoretical curves obtained from the simultaneous solution of Eqs. (10) and (17).

The results show that there is a satisfactory agreement of experiments and theory for relatively low speeds of $V/w_{0C} \leq 0.75$. However, deviations of the experimental data from the theory increase dramatically for higher V/w_{0C}, where the theory underpredicts the thrust performance of flapping wings.

V. Conclusions

A systematic review of recent applications of actuator disk theory to flapping wings of insects and birds has been presented. Unlike biological systems, flapping-wing aerodynamics can be studied explicitly on man-made flapping wings, since the input parameters specifying their kinematics and structures can be placed under full experimenter control.

The stroke-averaged thrust force measurements were conducted using 25 cm flat, 25 cm cambered, and 74 cm flat flapping-wing models. These wings represent membrane, batten structures. In a series of tests at zero freestream velocity, the thrust variation with flapping frequency was investigated for three wings. The results show that the thrust coefficient is highest and remains almost constant over the studied range of frequency for the 25 cm cambered wing.

The flapping axis of flapping-wing models was aligned with the freestream in the wind tunnel and the thrust was measured with the input power held constant. To account for spatial and temporal variance in the wake behind the flapping wings, previous studies proposed an empirical correction for the velocity induced by the actuator disk in hover. In the present study, a new procedure for the determination of the correction factor for the actuator disk theory was developed using thrust measurements at a constant input power and zero angle of attack for a range of freestream speeds. Theoretically, the thrust force generated by the actuator disk does not depend on the input power, and experiments showed consistency with the theory.

The 25 cm cambered wing had the lowest induced power losses of 18% and the highest thrust coefficient. It is worth mentioning that the actuator disk model ignores profile drag and does not include tip losses due to a finite number of wings/blades. Thus, the 25 cm cambered wing showed much better induced power efficiency in comparison to the 74 and 25 cm flat wings. The implication of this result is that the initial geometry of membrane flapping wings plays an important role in their aerodynamic performance.

The numerical value for the correction factor for 25 cm cambered wing is close to the results obtained for the large insect and for the contrarotating propellers, implying that man-made flapping wings, insect wings, and propellers may have comparable aerodynamic efficiency. Further studies are needed to explain observed results.

Additional wind-tunnel experiments were conducted on the 25 cm flat wing with the angle of attack varying at $\alpha = 28, 56$, and 85°. The results show that there is a satisfactory agreement of experiments and theory for relatively low speeds of $V/w_{0C} \leq 0.75$. However, deviations of the experimental data from the theory increase dramatically for higher velocities, where the theory underpredicts the thrust performance of flapping wings.

Acknowledgments

The support of 2008 and 2009 U.S. Air Force Summer Faculty Fellowships Awarded to S. Shkarayev is gratefully acknowledged. The authors also would like to thank the other members of the Micro Air Vehicle Project at the University of Arizona for their contributions to this work: Roman Krashanitsa, Gunjan Maniar, and Malladi Bharani.

References

[1] Sane, S. P., "Review. The Aerodynamics of Insect Flight," *Journal of Experimental Biology*, Vol. 206, 2003, pp. 4191–4208. doi:10.1242/jeb.00663

[2] Rozhdestvensky, K. V., and Ryzhov, V. A., "Aerodynamics of Flapping-Wing Propulsors," *Progress in Aerospace Sciences*, Vol. 39, 2003, pp. 585–633. doi:10.1016/S0376-0421(03)00077-0

[3] Shyy, W., Berg, M., and Ljungqvist, D., "Flapping and Flexible Wings for Biological and Micro Air Vehicles," *Progress in Aerospace Sciences*, Vol. 35, 1999, pp. 455–505. doi:10.1016/S0376-0421(98)00016-5

[4] Taylor, G. K., "Mechanics and Aerodynamics of Insect Flight Control," *Biological Reviews of the Cambridge Philosophical Society*, Vol. 76, 2001, pp. 449–471.

[5] Ansari, S. A., Zbikowski, R., and Knowles, K., "Aerodynamic Modeling of Insect-Like Flapping Flight for Micro Air Vehicles," *Progress in Aerospace Sciences*, Vol. 42, 2006, pp. 129–172. doi:10.1016/j.paerosci.2006.07.001

[6] Shyy, W., Lian, Y., Tang, J., Liu, H., Trizila, P., Stanford, B., Bernal, L., Cesnik, C., Friedmann, P., and Ifju, P., "Computational Aerodynamics of Low Reynolds Number Plunging, Pitching and Flexible Wings for MAV Applications," 46th AIAA Aerospace Sciences Meeting and Exhibit, AIAA Paper 2008-523, Reno, NV, 7–10 Jan. 2008.

[7] McCormick, B. W., Jr., *Aerodynamics of V/STOL Flight*, Dover, Mineola, NY, 1999, p. 328.

[8] Stepniewski, W. Z., and Keys, C. N., *Rotary-Wing Aerodynamics*, Dover, Mineola, NY, 1984, p. 640.

[9] Rankine, W. J., "On the Mechanical Principles of the Action of Propellers," *Transactions of the Institution of Naval Architects*, Vol. 6, 1865, pp. 13–39.

[10] Froude, R. E., "On the Part Played in Propulsion by Differences of Fluid Pressure," *Transactions of the Institution of Naval Architects*, Vol. 30, 1889, pp. 390–409.

[11] Glauert, H., *A General Theory of Autogyro*, Scientific Research Air Ministry, Research and Memoranda No. 1111, London, 1926, pp. 558–593.

[12] Osborne, M. F. M., "Aerodynamics of Flapping Flight with Application to Insects," *Journal of Experimental Biology*, Vol. 28, 1951, pp. 221–245.

[13] Pennycuick, C. J., "Mechanics of flight," *Avian Biology*, Academic Press, edited by, D. S. Farner, and J. R. King, New York, Vol. 5, 1975, pp. 1–75.

[14] Ellington, C. P., "The Aerodynamics of Hovering Insect Flight V: A Vortex Theory," *Philosophical Transactions of the Royal Society of*

London, Series B: Biological Sciences, Vol. 305, 1984, pp. 115–44.

[15] Willmot, A. P., and Ellington, C. P., "The Mechanics of Flight in Manduca Sexta II: Aerodynamic Consequences of Kinematic and Morphological Variation," *Journal of Experimental Biology*, Vol. 200, 1997, pp. 2723–2745.

[16] Sunada, S., and Ellington, C. P., "A New Method for Explaining the Generation of Aerodynamic Forces in Flapping Flight," *Mathematical Methods in the Applied Sciences*, Vol. 24, 2001, pp. 1377–1386. doi:10.1002/mma.186

[17] Templin, R. J., "The spectrum of animal flight: insects to pterosaurs,". *Progress in Aerospace Sciences*, Vol. 36, 2000, pp. 393–436. doi:10.1016/S0376-0421(00)00007-5

[18] Bomphrey, R. J., Taylor, G. K., Lawson, N. J., and Thomas, A. L. R., "Digital Particle Image Velocimetry Measurements of the Downwash Distribution of a Desert Locust Schistocerca Gregaria," *Journal of the Royal Society Interface*, Vol. 3, 2006, pp. 311–317. doi:10.1098/rsif.2005.0090

[19] Kline, S. J., and McClintock, F. A., "Describing Uncertainties in Single-Sample Experiments," *Mechanical Engineering*, Vol. 75, No. 1, 1953, pp. 3–8.

[20] Shkarayev, S., Silin, B., Abate, G., and Albertani, R., "Aerodynamics of Cambered Membrane Flapping Wings," 47th AIAA Aerospace Sciences Meeting, AIAA Paper 2010-0058, Orlando, FL, 4–7 Jan. 2010.

[21] Singh, B., and Chopra, I., "Insect-Based Hover-Capable Flapping Wings for Micro Air Vehicles: Experiments and Analysis," *AIAA Journal*, Vol. 46, No. 9, Sept. 2008, pp. 2115–2135. doi:10.2514/1.28192

[22] Du, G., and Sun, M., "Effects of Unsteady Deformation of Flapping Wings on Its Aerodynamic Forces," *Applied Mathematics and Mechanics*, Vol. 29, 2008, pp. 731–743. doi:10.1007/s10483-008-0605-9

[23] Shkarayev, S., Moschetta, J.-M., and Bataille, B., "Aerodynamic Design of Micro Air Vehicles for Vertical Flight," *Journal of Aircraft*, Vol. 45, 2008, pp. 1715–1724. doi:10.2514/1.35573

E. Livne
Associate Editor